Performance of DFT for C_{60} Isomerization Energies: A Noticeable Exception to Jacob's Ladder

Amir Karton,[a,*] Simone L. Waite,[b] and Alister J. Page[b]

[a]School of Molecular Sciences, The University of Western Australia, Perth, WA 6009, Australia.
[b]School of Environmental and Life Sciences, The University of Newcastle, Callaghan, NSW 2308, Australia.

ABSTRACT

The ability to accurately calculate relative energies of fullerenes is important in many areas of computational nanotechnology. Due to the large size of fullerenes, their relative energies cannot normally be calculated by means of high-level ab initio procedures, and therefore density functional theory (DFT) represents a cost-effective alternative. In an extensive benchmark study, we calculate the electronic energies of eight C_{60} isomers by means of the high-level G4(MP2) composite procedure. G4(MP2) isomerization energies span a wide range between 307.5–1074.0 kJ mol^{-1}. We use this benchmark data to assess the performance of DFT, double-hybrid DFT (DHDFT), and MP2-based ab initio methods. Surprisingly, functionals from the second and third rungs of Jacob's Ladder (i.e., GGA and meta-GGA functionals) significantly and systematically outperform hybrid and hybrid-meta-GGA functionals, which occupy higher rungs of Jacob's Ladder. In addition, DHDFT functionals do not offer a substantial improvement over meta-GGA functionals, with respect to isomerization energies. Overall, the best performing functionals with mean absolute deviations (MADs) below 15.0 kJ mol^{-1} are (MADs given in parenthesis) the GGA N12 (14.7); meta-GGAs M06-L (10.6), M11-L (10.8), MN15-L (11.9), and TPSS-D3BJ (12.8); and the DHDFT functionals B2T-PLYP (9.3), mPW2-PLYP (9.8), B2K-PLYP (12.1), and B2GP-PLYP (12.3 kJ mol^{-1}). In light of these results, we recommend the use of meta-GGA functionals for the calculation of fullerene isomerization energies. Finally, we show that inclusion of very small percentages of exact Hartree–Fock exchange (3–5%) slightly improves the performance of the GGA and meta-GGA functionals. However, their performance rapidly deteriorates with the inclusion of larger percentages of exact Hartree–Fock exchange.

Keywords: Buckminsterfullerene; density functional theory; coupled cluster theory; G4(MP2) theory.

Cite as:
A. Karton, S. L. Waite, A. J. Page, *J. Phys. Chem. A*, 123, 257–266 (2019). https://doi.org/10.1021/acs.jpca.8b10240

Corresponding Author. Tel.: +61 8 6488 3139. Fax: +61 8 6488 7330. E-mail address: amir.karton@uwa.edu.au (A. Karton).

1. Introduction

Isomerization energies are fundamental thermochemical quantities that are required for comparing the thermodynamic stability of isomers. Fullerene isomerization energies are of particular importance for prediction of their thermodynamic stability (and assessment of the kinetic stability).[1,2,3,4,5,6] Over the past two decades density functional theory (DFT) has become the most applied quantum chemical method for medium-sized chemical systems due to its attractive accuracy-to-computational cost ratio (medium-sized systems here refer to molecules for which high-level ab initio methods cannot be routinely applied, i.e., with over 50 non-hydrogen atoms). The approximations for the exchange-correlation functional can be classified according to their rung on Perdew's 'Jacob's Ladder':[7] (1) the local density approximation; (2) pure generalized gradient approximation (GGA) employing both the local density and the reduced density gradient; (3) the meta-GGAs which additionally employ the kinetic energy density; (4) the hybrid-GGAs and hybrid-meta-GGAs which in addition involve the occupied orbitals; and (5) the double-hybrid functionals which additionally employ the virtual orbitals.

Numerous benchmark studies have shown that the performance of DFT functionals improves along the rungs of Jacob's Ladder,[8,9,10,11,12,13,14,15,16,17,18,19,20] and this is also true for isomerization energies of carbon rich molecules.[17,18,19,20] This has been found to be the case for (i) isomerization energies in polycyclic aromatic hydrocarbons,[17] (ii) conjugated → non-conjugated isomerizations in dienes,[18] (iii) C_8H_8 structural isomerizations,[19] and (iv) linear–cyclic isomerization energies in small carbon clusters.[20] Given the fundamental importance of Jacob's Ladder in DFT, it is important to identify cases for which this hierarchy does not hold, and if possible, arrive at guidelines with regard to when this might occur. Identifying such cases is important for both users and developers of DFT.

In the present work, we introduce a representative database of high-level C_{60} isomerization energies (to be known as the iso-C60 database). The isomers in the iso-C60

database are shown in Figure 1. The database covers a broad spectrum of structures with relative energies ranging between 307.5–1074.0 kJ mol^{-1}, relative to the most stable Buckminsterfullerene isomer. Reference isomerization energies at the CCSD(T)/CBS level (i.e., coupled cluster energy with single, double, and quasiperturbative triple excitations at the complete basis-set limit) are approximated by means of the high-level G4(MP2) composite procedure. These benchmark values allow us to assess the performance of more approximate DFT and MP2-based ab initio procedures for the isomerization energies. Specifically, we examine the performance of a variety of contemporary DFT procedures across all rungs of Jacob's Ladder. One important finding is that inclusion of even small amounts of exact Hartree–Fock exchange in the functional form results in a significant deterioration in performance of GGA and meta-GGA functionals. In addition, the high-level double-hybrid functionals do not offer a noticeable improvement over the computationally economical meta-GGA functionals. Therefore, the performance of DFT methods does not exhibit the normal improvement along the rungs of Jacob's Ladder with respect to C_{60} isomerization energies.

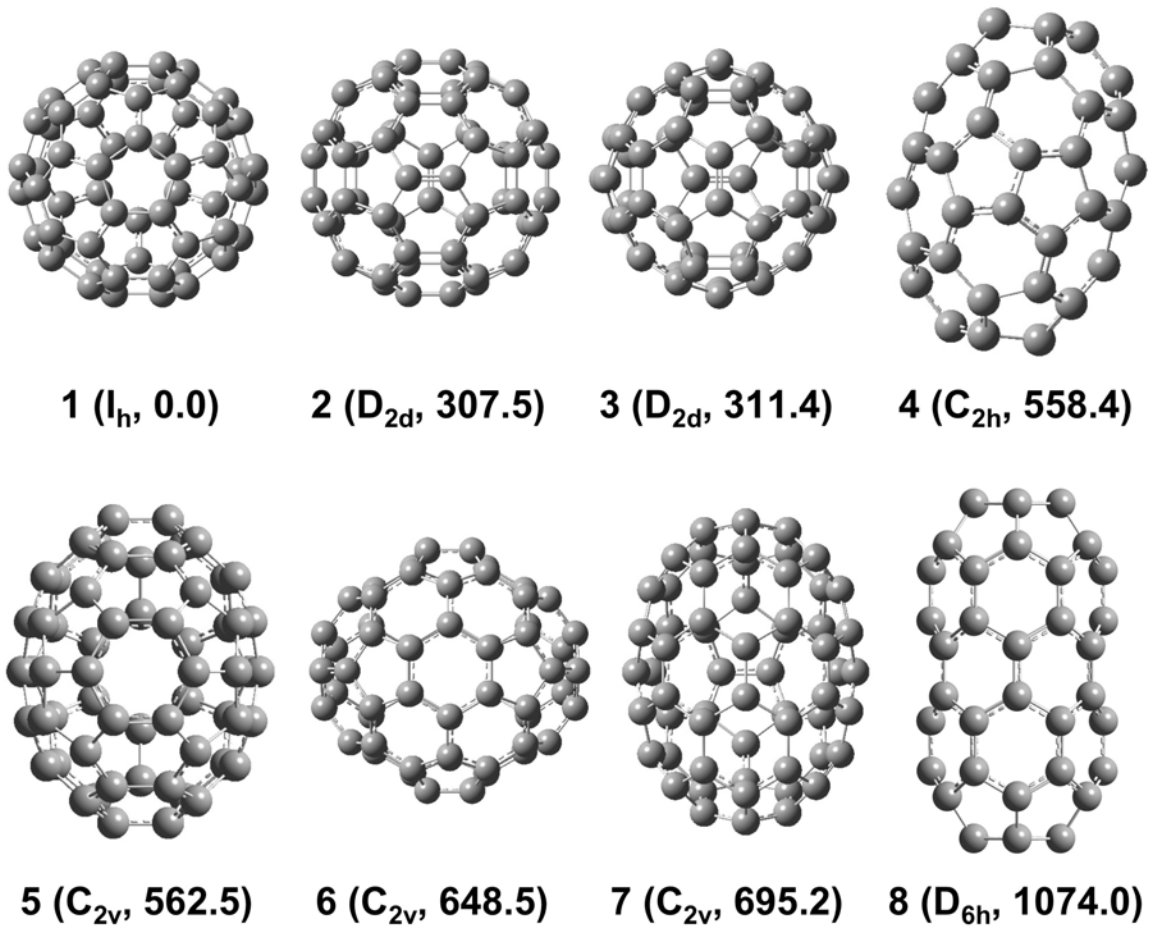

Figure 1. Optimized structures of the C_{60} isomers in the iso-C60 database. The point-group symmetry and the relative G4(MP2) isomerization energy in kJ mol^{-1} are given in parenthesis.

2. Computational Methods

In order to obtain reliable reference relative energies for the C_{60} isomers, calculations have been carried out using the high-level, ab initio G4(MP2) method,[21,22] which provides a cost-effective approach for approximating the CCSD(T)/CBS energy.[23] In particular, G4(MP2) theory uses an additivity-based formula of the form:

$$E[\text{G4(MP2)}] = E[\text{CCSD(T)/6-31G(d)}] + \Delta E(\text{MP2}) + \Delta E(\text{HF}) \quad (1)$$

where the basis-set-correction terms are given by

$$\Delta E(\text{MP2}) = E[\text{MP2/G3MP2LargeXP}] - E[\text{MP2/6-31G(d)}] \quad (2)$$

$$\Delta E(\text{HF}) = E[\text{HF/\{T,Q\}}] - E[\text{HF/G3LargeXP}] \quad (3)$$

Here, HF/{T,Q} indicates extrapolation of the HF energy from truncated versions of the aug-cc-pVTZ and aug-cc-pVQZ basis sets.

It should be pointed out that ideally, we should be using a higher-level composite ab initio method such as W1-F12 which approximates the CCSD(T) energy closer to the basis set limit for calculating the C_{60} isomerization energies;[23,24] however, these calculations proved beyond our computational resources. Nevertheless, the G4(MP2) isomerization energies should be of sufficient accuracy for the purpose of benchmarking DFT and MP2-based procedures due to a large degree of systematic error cancelation between reactants and products.[16,17,25,26] For example, for isomerization energies of ortho, meta, and para carboranes ($C_2B_{10}H_{12}$) the deviations between G4(MP2) and W1-F12 amount to less than 1 kJ mol^{-1}.[27]

The DFT exchange-correlation functionals considered in the present study (ordered by their rung on Jacob's Ladder)[7] are given in Table 1. Empirical D3 dispersion corrections[28,29,30] are included in some cases using the finite Becke–Johnson[31] and zero-damping potentials (denoted by the suffix -D3BJ and -D3, respectively). We note that the suffix -D in B97-D and ωB97X-D indicates the original dispersion correction.

Table 1. DFT exchange-correlation functionals considered in the present work.

Type[a]	Functionals
GGA	BLYP,[32,33] B97-D,[34] HCTH407,[35] PBE,[36] BP86,[32,37] BPW91,[33,38] SOGGA11,[39] N12[40]
MGGA	M06-L,[41] TPSS,[42] τ-HCTH,[43] VSXC,[44] BB95,[45] M11-L,[46] MN12-L,[47] MN15-L[48]
HGGA	BH&HLYP,[49] B3LYP,[32,50,51] B3P86,[50,37] B3PW91,[50,38] PBE0,[52] B97-1,[53] B98,[54] X3LYP,[55] SOGGA11-X,[56] APF,[57] APFD,[57] mPW1PW91,[58,38] mPW1LYP,[58,32] mPW1PBE,[58,36] HSE03,[59] HSE06[60]
HMGGA	M05,[61] M05-2X,[62] M06,[63] M06-2X,[63] M06-HF,[63] M08HX,[64] MN15,[48] BMK,[65] B1B95,[32,45] TPSSh,[66] τ-HCTHh,[43] PW6B95[67]
DH	B2-PLYP,[68] mPW2-PLYP,[69] PBE0DH,[70] PBEQIDH,[71] B2GP-PLYP,[72] B2K-PLYP,[73] B2T-PLYP,[73] DSD-BLYP,[74] DSD-PBEP86[75,76]
RS	ωB97,[77] ωB97X,[77] ωB97X-D,[78] M11,[79] N12SX,[80] MN12SX,[80] CAM-B3LYP,[81] LC-ωHPBE,[82] LC-ωPBE,[83] LC-BLYP, LC-PBE, LC-BP86, and LC-BPW91[84]

[a]GGA = generalized gradient approximation, HGGA = hybrid-GGA, MGGA = meta-GGA, HMGGA = hybrid-meta-GGA, DH = double hybrid, RS = range-separated.

In addition, the performance of approximate ab initio methods is also assessed. We consider the performance of the following standard ab initio methods: MP2, SCS-MP2,[85] SOS-MP2,[86] SCS(MI)-MP2,[87] SCSN-MP2,[88] SCS-MP2-vdW,[89] S2-MP2.[90] All the DFT, DHDFT, and MP2 calculations were carried out in conjunction with the Def2-TZVPP basis set.[91] The geometries of all structures have been obtained at the PBE-D3/Def2-TZVPP level of theory and taken from reference 1. All ab initio calculations involved in the G4(MP2) procedure were calculated using Molpro 2016.[92,93] All DFT and DHDFT calculations were performed using the Gaussian 16 program suite.[94]

3. Results and Discussion

3.1. Overview of the benchmark isomerization energies in the iso-C60 database. The isomers in the iso-C60 database are shown in Figure 1 along with the G4(MP2) isomerization energies (ΔE_{iso}) relative to the well-known I_h symmetry buckminsterfullerene isomer. This highly symmetric isomer involves 12 pentagons completely surrounded by hexagons, and is the only isomer of C_{60} to satisfy the isolated pentagon rule. The next two isomers (**2** and **3**) are structurally similar, e.g., they both involve six fulvalene units surrounded by hexagons, and lie close in energy to one another (namely, at the G4(MP2) level ΔE_{iso} = 307.5 and 311.4 kJ mol^{-1}, respectively). The next two isomers (**4** and **5**) are energetically similar ellipsoids with ΔE_{iso} = 558.4 and 562.5 kJ mol^{-1}, respectively. Similarly to isomer **1**, isomers **6** and **7** involve 12 pentagons, however, since these pentagons are not completely surrounded by hexagons these isomers are not spherical and are highly energetic with ΔE_{iso} = 648.5 and 695.2 kJ mol^{-1}, respectively. Isomer **8**, which may be essentially described as a capped nanotube, is the highest-energy C_{60} isomer with ΔE_{iso} = 1074.0 kJ mol^{-1}. We note that ideally it would have been good to include additional C_{60} isomers in the iso-C60 database; however, due to the high computational cost associated with the CCSD(T)/6-31G(d) calculations the present study can only consider highly symmetric isomers, and even these calculations strained our computational resources to the limit. For example, the CCSD(T)/6-31G(d) calculation for isomer **2** (in D_{2d} symmetry) ran for 31 days on 4 Intel Xeon E5-2670v2 cores (at 3.1 GHz) with 256 GB of RAM and 2 TB of solid-state disk.

3.2. Relative errors for the DFT and ab initio procedures for the isomerization energies in the iso-C60 database. As shown in Section 3.1, the isomerization energies in the iso-C60 database spread over a wide range, namely between 307.5 and 1074.0 kJ mol^{-1}. It is therefore instructive to begin by examining the relative errors in the isomerization energies. Table S1 of the

Supporting Information lists the relative errors for all the methods that were considered in the present work. Inspection of these results reveals that for 67 of the 115 methods considered here the maximum relative errors exceed 10%. Table 2 summarizes the relative errors for the remaining 48 methods for which the maximum relative error is smaller than 10%.

Table 2. Minimum and maximum relative errors for DFT and SCS-MP2 isomerization energies of fullerene isomers in the iso-C60 database. The isomerization energy for which the minimum or maximum error is obtained is given in parenthesis. Only functionals with maximum relative errors ≤ 10.0% are listed here (for the complete set see Table S1 of the Supporting Information). Functionals with maximum relative errors ≤ 5.0% are listed in green font, functionals with minimum relative errors ≥ 5.0% are listed in red font.

Type[a]	Functional	Min[b]	Max[b]
GGA	N12	0.2 (3)	4.6 (5)
	BLYP-D3BJ	0.6 (3)	5.1 (5)
	HCTH407	0.3 (8)	5.4 (5)
	PBE-D3BJ	1.2 (3)	6.1 (5)
	BLYP	0.4 (8)	6.2 (5)
	BPW91	0.7 (8)	6.2 (5)
	BLYP-D3	1.8 (8)	6.3 (5)
	BP86	1.0 (8)	6.5 (5)
	PBE-D3	1.8 (3)	6.6 (5)
	PBE	1.5 (8)	6.7 (5)
	B97-D	2.3 (8)	7.1 (5)
	SOGGA11	4.7 (3)	10.0 (7)
MGGA	TPSS-D3BJ	0.6 (3)	3.9 (5)
	M06-L	0.2 (7)	4.1 (8)
	M11-L	0.0 (5)	4.2 (8)
	MN15-L	0.3 (7)	4.5 (3)
	M06L-D3	0.1 (7)	4.6 (8)
	TPSS	0.4 (3)	4.6 (5)
	TPSS-D3	0.3 (3)	4.6 (5)
	VSXC	0.3 (3)	4.6 (8)
	τ-HCTH	0.3 (3)	4.9 (5)
	BB95	3.5 (3)	8.4 (5)
	MN12-L	4.0 (5)	9.1 (8)
HGGA	B3PW91-D3BJ	6.5 (6)	8.5 (8)
	B3PW91-D3	5.5 (6)	8.7 (8)
	APF-D	5.9 (2)	9.2 (8)
	B3LYP-D3BJ	6.6 (6)	9.8 (8)
HMGGA	TPSSh-D3	1.4 (5)	5.1 (8)
	TPSSh-D3BJ	2.8 (5)	5.4 (3)
	TPSSh	1.4 (5)	6.5 (8)

	τ-HCTHh	2.6 (6)	7.8 (8)
	M05-D3	5.0 (2)	8.5 (8)
	M05	5.0 (2)	9.0 (8)
	M06	4.9 (2)	9.2 (8)
	M06-D3	5.1 (2)	9.2 (8)
DH	B2-PLYP-D3BJ	0.7 (4)	3.9 (8)
	B2-PLYP	0.9 (4)	4.0 (5)
	B2-PLYP-D3	1.2 (4)	4.1 (5)
	B2T-PLYP	0.3 (6)	4.6 (3)
	B2GP-PLYP	0.3 (4)	4.7 (3)
	B2GP-PLYP-D3	0.2 (4)	4.7 (3)
	mPW2-PLYP	0.1 (5)	5.2 (3)
	B2GP-PLYP-D3BJ	0.4 (6)	5.2 (3)
	B2K-PLYP	0.1 (6)	5.5 (3)
	DSD-BLYP	1.8 (4)	6.7 (8)
	DSD-PBEP86	0.8 (4)	7.0 (8)
	PBEQI-DH	2.1 (8)	8.0 (3)
Ab initio	SCS(MI)-MP2	0.9 (6)	9.1 (3)
	SCS-MP2opt	0.4 (7)	9.9 (3)

[a]Footnote *a* to Table 1 applies here. [b]The isomerization energy for which the minimum and maximum error is obtained is given in parenthesis (see Figure 1).

Remarkably, with no exception *all* of the GGA and meta-GGA functions result in maximum relative errors smaller than 10%. Even more remarkably, for nearly all of the considered MGGA functionals (i.e., 9 out of 11 functionals) the maximum relative errors are below 5% (Table 2).

For the GGAs we obtain maximum relative errors ranging between 4.6% (N12) and 10% (SOGGA11). Where in all cases but one the maximum relative error is obtained for the **1** → **5** isomerization. It is interesting to note that GGA methods systematically struggle with this isomerization reaction, rather than with isomerization reactions which are associated with a larger isomerization energy (Figure 1). This point is important since for functionals from higher rungs of Jacob's Ladder the maximum relative error is usually obtained for the **1** → **8** isomerization. Of the GGA functionals, N12 shows the best performance with a minimum relative error of 0.2% (for the **1** → **3** isomerization) and a maximum relative error of 4.6% (for the **1** → **5**

isomerization). All the other GGA functionals result in maximum relative errors larger than 5.0%.

Inclusion of the kinetic energy density in the meta-GGA procedures significantly improves the performance. For example, nine out of the eleven considered MGGAs result in maximum relative errors below 5.0%. Particularly good performance, with maximum relative errors of about 4%, is obtained for (maximum relative errors are given in parenthesis): TPSS-D3BJ (3.9%), M06-L (4.1%), and M11-L (4.2%).

Inclusion of exact exchange (EXX) in the HGGA functionals, on the other hand, results in significant deterioration in performance. This is illustrated by the fact that, of the 26 considered HGGA functionals considered here, only four result in maximum relative errors smaller than 10%, namely B3LYP-D3BJ (9.8%), APFD (9.2%), B3PW91-D3 (8.7%), and B3PW91-D3BJ (8.5%). However, in all these cases the minimum relative errors are larger than 5%. Thus, it is evident that inclusion of exact HF exchange results in a significant deterioration in performance across the board (see Section 3.4 for further details).

Overall, the hybrid-meta-GGAs also result in poor performance relative to the GGAs and meta-GGAs. For example, eight of the 25 considered HMGGA functionals result in maximum relative errors smaller than 10%, and none of these result in minimum relative errors smaller than 5%. The best performing HMGGA is TPSSh, with maximum relative errors of 5.1% (TPSSh-D3) and 5.4% (TPSSh-D3BJ).

Particularly large maximum relative errors of about 25–40% are obtained for the considered range separated (RS) functionals, with the exception of N12SX and MN12SX (Table S1 of the Supporting Information). The best performing RS functionals are (maximum relative errors are given in parenthesis): N12SX (11.2%), MN12SX (11.2%), and CAM-B3LYP-D3BJ (23.6%). We note that the minimum relative errors significantly exceed 5% in all cases (Table S1).

The DHDFT functionals are the only functionals above the third rung of Jacob's Ladder that achieve good performance. However, it is important to note that they do not offer an improvement over the MGGA functionals. The best performing DH functional is B2-PLYP-D3BJ with a maximum relative error of 3.9%. This performance is similar to that of the MGGA functional TPSS-D3BJ (Table 2). Of the 13 DH functionals, only one method (PBE0-DH) attains a maximum relative error above 10%.

Finally, we note that of the considered HF- and MP2-based methods, only SCS(MI)-MP2 attains a maximum relative error below the 10% threshold. The other methods result in maximum relative errors ranging between 15.2% (SOS-MP2) and 55.9% (HF-D3BJ).

3.3. Absolute errors for the DFT and ab initio procedures for the isomerization energies in the iso-C60 database. The relative errors discussed in Section 3.2 indicate that the GGA, meta-GGA, and DHDFT procedures significantly outperform hybrid and hybrid-meta GGA methods. In this section we will examine the statistical analysis of the absolute errors. Figure 2 gives an overview of the root-mean-square deviations (RMSDs) for the 104 DFT methods that were considered in this work. Inspection of this figure reveals that the hybrid-GGAs, hybrid-meta-GGAs, and range separated functionals result in very poor performance. With the exception of TPSSh and τ-HCTHh, the RMSDs for these functionals range between ~50 and well over 100 kJ mol^{-1}. In contrast, nearly all of the GGA and meta-GGA functionals result in RMSDs of ~25 kJ mol^{-1}.

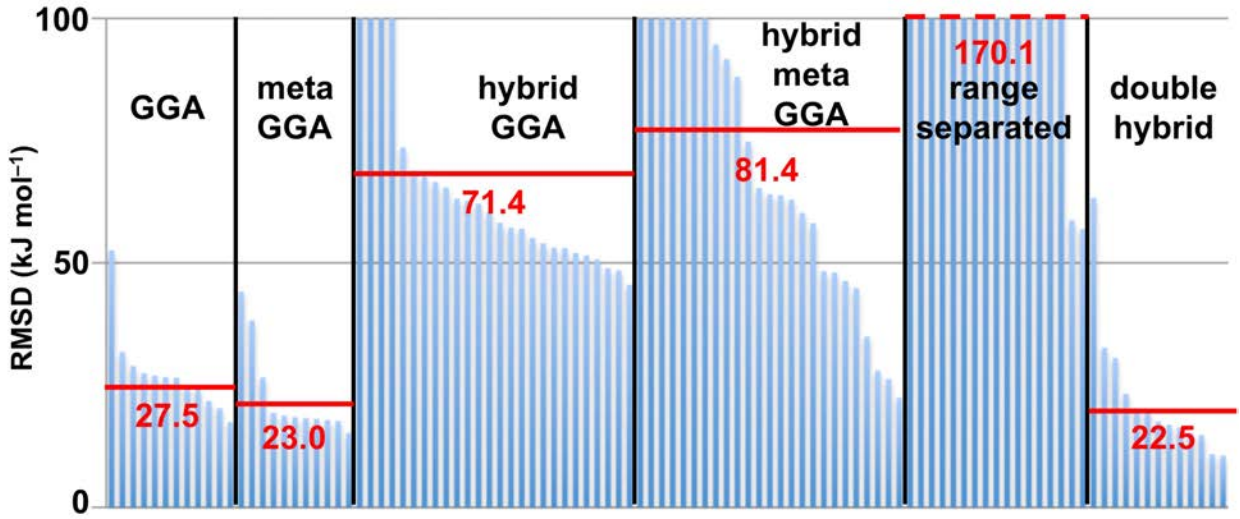

Figure 2. Root-mean-square deviations (RMSDs) for all of the DFT procedures over the isomerization energies in the iso-C60 database relative to G4(MP2) reference values (in kJ mol^{-1}). The average RMSD across all functionals from each rung of Jacob's Ladder is shown in red. See Table 2 (and Table S2 of the Supporting Information) for the specific RMSD for each functional.

Table 3 gives an overview of the performance of the DFT functionals with RMSDs < 50.0 kJ mol^{-1}. Table S2 of the Supporting Information gives an overview of the performance for all the methods that were considered in the present work. The second-order GGA functional SOGGA11 is the only GGA method with and RMSD larger than 50.0 kJ mol^{-1} (namely, 52.6 kJ mol^{-1}). The rest of the GGAs show fairly good performance with RMSDs ranging between 17.5 (N12) and 31.8 (B97-D) kJ mol^{-1}. All the GGAs tend to systematically underestimate the isomerization energies. The best performing GGAs are N12 and HCTH407 with RMSDs of 17.5 and 20.3 6 kJ mol^{-1}, respectively.

Table 3. Statistical analysis for the performance of DFT, DHDFT, and ab initio procedures for the isomerization energies in the iso-C60 database (in kJ mol^{-1}). The G4(MP2) reference values are given in Figure 1. Only functionals with RMSDs < 50 kJ mol^{-1} are listed, see Table S2 of the Supporting Information for the entire set of functionals.

Type[a]	Method	RMSD[b]	MAD[b]	MSD[b]	LND[b,c]	LPD[b,c]
GGA	N12	17.5	14.7	–11.6	–26.3 (7)	10.1 (8)
	HCTH407	20.3	16.4	–15.6	–31.4 (7)	2.8 (8)
	BLYP-D3BJ	21.8	19.2	–19.2	–30.1 (7)	N/A
	BLYP	24.3	20.9	–19.6	–35.2 (7)	4.3 (8)
	BPW91	24.6	21.1	–21.1	–36.7 (7)	N/A

	BP86	26.6	23.4	–23.4	–39.4 (7)	N/A
	BLYP-D3	26.7	24.1	–24.1	–37.9 (7)	N/A
	PBE-D3BJ	27.0	24.2	–24.2	–38.2 (7)	N/A
	PBE	27.5	24.5	–24.5	–40.7 (7)	N/A
	PBE-D3	29.0	26.2	–26.2	–41.6 (7)	N/A
	B97-D	31.8	29.1	–29.1	–45.6 (7)	N/A
MGGA	TPSS-D3BJ	15.3	12.8	–12.3	–23.2 (7)	1.8 (3)
	M06-L	17.7	10.6	8.7	–5.3 (5)	44.4 (8)
	TPSS	17.9	15.4	–12.3	–26.2 (7)	11.1 (8)
	M11-L	18.1	10.8	10.7	–0.3 (5)	45.0 (8)
	TPSS-D3	18.3	15.1	–15.1	–27.8 (7)	N/A
	τ-HCTH	18.5	15.9	–11.7	–27.3 (5)	14.6 (8)
	MN15-L	18.8	11.9	11.9	N/A	46.4 (8)
	M06-L-D3	19.4	11.4	9.9	–4.8 (5)	49.0 (8)
	VSXC	26.6	22.1	–22.1	–49.2 (8)	N/A
	BB95	38.3	35.3	–35.3	–52.8 (7)	N/A
	MN12-L	44.2	35.9	35.9	N/A	98.1 (8)
HGGA	B3PW91-D3	45.6	39.3	39.3	N/A	92.9 (8)
	B3PW91-D3BJ	48.5	43.7	43.7	N/A	90.9 (8)
	APF-D	49.0	42.1	42.1	N/A	99.2 (8)
HMGGA	TPSSh-D3	22.5	16.0	16.0	N/A	54.4 (8)
	TPSSh-D3BJ	26.3	22.9	22.9	N/A	54.1 (8)
	TPSSh	28.0	18.9	18.9	N/A	69.3 (8)
	τ-HCTHh	35.0	25.2	25.2	N/A	84.1 (8)
	M05-D3	44.9	38.3	38.3	N/A	91.8 (8)
	M05	46.4	39.1	39.1	N/A	96.2 (8)
	M06	48.1	40.4	40.4	N/A	99.2 (8)
	M06-D3	48.4	40.9	40.9	N/A	99.3 (8)
DH	B2T-PLYP	10.6	9.3	–1.1	–16.5 (8)	14.3 (3)
	mPW2-PLYP	10.9	9.8	9.7	–0.5 (5)	16.2 (3)
	B2GP-PLYP	14.8	12.3	–4.5	–29.2 (8)	14.7 (3)
	B2K-PLYP	15.3	12.1	–1.8	–30.8 (8)	17.2 (3)
	B2GP-PLYP-D3	16.4	13.1	–5.6	–34.0 (8)	14.6 (3)
	B2GP-PLYP-D3BJ	16.9	13.1	–4.0	–36.3 (8)	16.3 (3)
	B2-PLYP	17.6	15.1	–10.7	–31.6 (8)	9.9 (3)
	B2-PLYP-D3BJ	19.9	16.1	–10.5	–42.0 (8)	11.9 (3)
	B2-PLYP-D3	20.3	17.0	–12.7	–39.9 (8)	9.8 (3)
	PBEQI-DH	23.3	23.1	23.1	N/A	25.9 (4)
	DSD-PBEP86	30.6	20.2	–14.8	–75.3 (8)	11.1 (3)
	DSD-BLYP	32.7	25.1	–20.1	–72.0 (8)	11.0 (3)
Ab initio	SCS-MP2opt	20.9	18.3	5.5	–29.2 (8)	30.7 (3)
	SCS(MI)-MP2	29.1	23.9	–7.2	–57.9 (8)	28.3 (3)
	SCSN-MP2	25.9	22.3	19.0	–11.4 (5)	42.1 (3)

[a]Footnote *a* to Table 1 applies here. [b]RMSD = root-mean-square deviation, MAD = mean-absolute deviation, MSD = mean-signed deviation, LND = largest negative deviation, LPD = largest positive deviation. [c]The isomerization reaction is given in parenthesis (see Figure 1).

Inclusion of the kinetic energy density in the MGGA procedures improves predicted isomerization energies. With the exception of three methods (BB95, MN12-L and VSXC), all the MGGAs result in RMSDs smaller than 20 kJ mol^{-1}. In particular, TPSS-D3BJ results in a remarkably small RMSD of 15.3 kJ mol^{-1}. These results are particularly impressive when considering that the reference G4(MP2) isomerization energies range between 307.5–1074.0 kJ mol^{-1}. That is, these RMSDs amount to about 1.4% of the largest isomerization energy. In contrast to the GGAs, the MGGAs do not underestimate the isomerization energies across the board. Some MGGAs (e.g., TPSS, τ-HCTH, VSXC, and BB95) tend to systematically underestimate the isomerization energies, whilst the Truhlar MGGAs (M06-L, M11-L, MN12-L, and MN15-L) tend to systematically overestimate the isomerization energies.

The hybrid-GGA functionals show exceptionally poor performance with most RMSDs being well over 50 kJ mol^{-1} (Table S2 of the Supporting Information). The three functionals with RMSDs < 50 kJ mol^{-1} are B3PW91-D3, B3PW91-D3BJ, and APF-D. However, the RMSDs for these methods all exceed 45 kJ mol^{-1}. Figure 3 shows that there is a general correlation between the amount of exact HF exchange in the HMGGAs and the RMSDs. Functionals with ~20% of exact exchange (e.g., B3LYP, B97-1, and B98) attain RMSD of 50–60 kJ mol^{-1}, functionals with ~25% of exact exchange (e.g., PBE0 and mPW1PW91) attain RMSD of 65–70 kJ mol^{-1}, and functionals with over 40% of exact exchange (e.g., SOGGA11-X and BH&HLYP) attain RMSDs of over 100 kJ mol^{-1}.

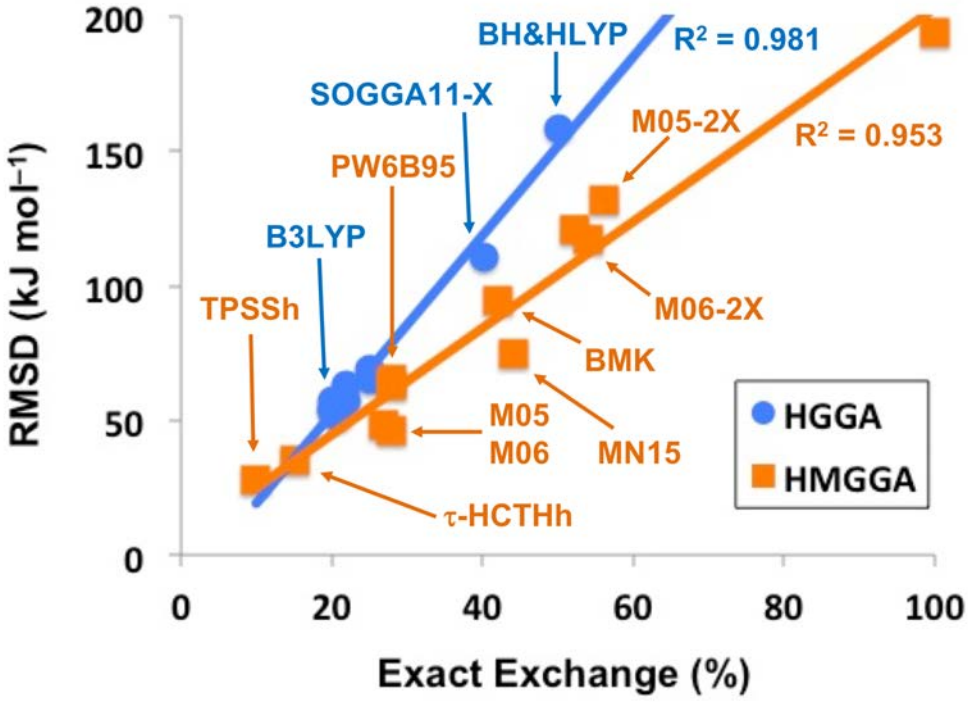

Figure 3. Linear relationship between the amount of exact exchange and the RMSD of the HGGA (blue line) and HMGGA (orange line) functionals.

The range-separated DFT functionals show significantly poorer performance compared with the global hybrids. For example, none of the range-separated functionals results in an RMSD smaller than 50 kJ mol^{-1}, and for most methods the RMSD exceeds 100 kJ mol^{-1} (Table S2 of the Supporting Information).

All of the double-hybrid functionals show good-to-excellent performance, with the exception of the parameter free PBE0-DH procedure which attains an RMSD > 50 kJ mol^{-1} (Figure 2 and Table S2 of the Supporting Information). The best performing DHDFT procedures are the older-generation B2T-PLYP and mPW2-PLYP functionals with RMSDs of 10.6 and 10.9 kJ mol^{-1}, respectively. It is noteworthy that B2T-PLYP results in a near-zero mean-signed-deviation of –1.1 kJ mol^{-1}. Finally, we note that B2GP-PLYP and B2K-PLYP also show very good performance with RMSDs of ~15 kJ mol^{-1}.

The RMSDs for the MP2-based ab initio methods span a wide range: from ~140 (MP2, SCSN-MP2, and SCS-MP2-vdW) to 25.9 (SCSN-MP2) kJ mol^{-1}. The SCS-MP2 procedure

shows poor performance with an RMSD of 88.2 kJ mol^{-1}. Optimizing the same-spin and opposite-spin scaling factors to minimize the RMSD over the iso-C60 dataset results in an RMSD of 20.9 (SCS-MP2opt, Table 3). However, we note that this does not offer an advantage over the best performing GGA and meta-GGA methods, which are computationally much more economical.

3.4. Optimal percentage of exact HF exchange. In the previous sections we have seen that inclusion of even moderate percentages of exact HF exchange in the functional form results in a significant deterioration in performance. Figure 3 shows the relationship between the amount of exact HF exchange and the RMSD of the HGGA and HMGGA functionals. Inspection of this Figure reveals two notable features:

- For both the HGGA and HMGGA there is a general correlation between the amount of exact HF exchange and the RMSD
- HMGGA procedures generally perform better than the HGGAs, albeit both procedures show poor performance

Let us consider, for example, the performance of the HMGGA functionals. Procedures with 10–15% of exact exchange (e.g., TPSSh and τ-HCTHh) result in RMSDs of 30–35 kJ mol^{-1}. Procedures with 27–28% of exact exchange (e.g., M06, PW6B95, and B1B95) result in RMSDs of 50–60 kJ mol^{-1}. Procedures with 40–50% of exact exchange (e.g., BMK, MN15, and M06-2X) result in RMSDs of 75–120 kJ mol^{-1}. The HGGA functionals show the same trend. For comparison, nearly all the GGA and MGGA procedures result in RMSDs below (or well below) 30 kJ mol^{-1}. Another key difference between the GGA/MGGA and HGGA/HMGGA procedures is that whilst the former tend to systematically underestimate the C_{60} isomerization energies (as

evident from negative MSDs), the latter overestimate the isomerization energies across the board (as evident from positive MSDs, Table 3).

To investigate this further, we chose two GGAs (BLYP and HCTH) and two MGGAs (τ-HCTH and TPSS) and we have scanned the percentage of exact HF exchange between 0–100%. Let us start by examining the performance of these functionals with 10–100% of exact exchange. The RMSDs over the iso-C60 dataset for these functionals with 10–100% EXX are depicted in Figure 4a. It can be seen that these functionals exhibit almost perfect linear correlation between the RMSD and percentage of EXX. This is demonstrated by squared correlation coefficients $R^2 > 0.9999$ for all four functionals. It is also evident that the RMSDs increase rapidly with the percentage of exact exchange, for example, for BLYP we obtain the following RMSDs (percentage of EXX given in parenthesis) 25.3 (10%), 56.9 (20%), 90.8 (30%), 158.4 (50%), and 320.2 (100%) kJ mol^{-1}. Similar results are obtained for the other functionals (Figure 4a).

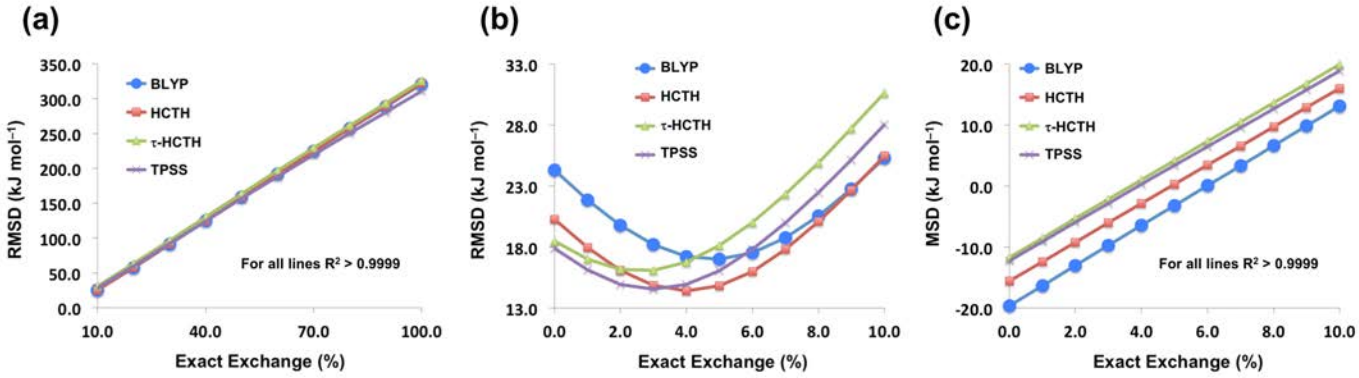

Figure 4. Dependence of the RMSDs (a and b) and MSDs (c) for the iso-C60 dataset on the exact exchange mixing coefficient for two GGA (BLYP and HCTH) and two meta-GGA (τ-HCTH and TPSS) functionals.

Let us move to the RMSDs over the range of 0–10% EXX. These results are given in Figure 4b. The four functionals exhibit a shallow minimum at very low percentages of EXX. Namely, at 5% (BLYP), 4% (HCTH), and 3% (τ-HCTH and TPSS). Inclusion of these admixtures of EXX reduces the RMSDs by 7.3 (BLYP), 5.9 (HCTH), 2.4 (τ-HCTH), and 3.3 (TPSS) kJ mol^{-1} relative

to the pure functionals. Thus, the most pronounced improvement in performance is obtained for BLYP, where inclusion of 5% of EXX reduces the RMSD from 24.3 to 17.0 kJ mol^{-1}. We note that this RMSD is comparable to that of the B2-PLYP DH functional at a significantly reduced computational cost.

As discussed in the previous section the GGA and MGGA procedures tend to systematically underestimate the C_{60} isomerization energies. Figure 4c gives the MSDs for the four functionals at EXX percentages of 0–10%. For all four functionals the MSD varies linearly with the percentage of EXX in the functional form. The MSD changes sign from negative to positive at 4–6% of exact HF exchange for the four functionals. This is consistent with the percentage of EXX which minimizes the RMSD (Fig. 4b).

3.5. Dispersion corrections. Table 4 gathers the differences in RMSD between the dispersion-corrected and uncorrected DFT functionals. We consider both the D3 correction with a zero-damping function (ΔD3 = RMSD(DFT) – RMSD(DFT-D3)) and the D3BJ correction with the finite Becke–Johnson damping function (ΔD3BJ = RMSD(DFT) – RMSD(DFT-D3BJ)). A positive ΔD3 (or ΔD3BJ) value indicates that the dispersion correction improves the performance of the functional, whereas a negative value indicates deterioration in performance. Inspection of Table 4 reveals that inclusion of either the D3 or D3BJ correction has a relatively minor effect on the performance of DFT for the C_{60} isomerization energies. With the exception of four functionals the dispersion corrections affect the RMSDs by less than 5.0 kJ mol^{-1}. In the four exceptions, the D3 correction improves the performance by 5.5 (TPSSh), 6.5 (B3LYP), 6.6 (BMK), and 7.6 (B3PW91) kJ mol^{-1}.

Table 4. Overview of the performance of various DFT functionals with and without empirical D3 and D3BJ dispersion corrections. The tabulated values are ΔD3 = RMSD(DFT) – RMSD(DFT-D3) and ΔD3BJ = RMSD(DFT) – RMSD(DFT-D3BJ) (in kJ mol^{-1}).[a]

Type[b]	Method	ΔD3	ΔD3BJ
GGA	BLYP	–2.4	2.5
	PBE	–1.5	0.5
MGGA	M06-L	–1.7	N/A
	TPSS	–0.4	2.6
HGGA	BH&HLYP	4.4	2.2
	B3LYP	6.5	4.2
	B3PW91	7.6	4.7
	PBE0	3.3	2.3
HMGGA	PW6B95	1.5	1.3
	M05	1.5	N/A
	M05-2X	–0.8	N/A
	M06	–0.3	N/A
	M06-2X	–1.7	N/A
	M06-HF	–1.0	N/A
	BMK	6.6	3
	B1B95	4.8	2.7
	TPSSh	5.5	1.7
RS	CAM-B3LYP	3.5	2.2
	LC-ωPBE	3.7	2.2
DH	B2-PLYP	–2.4	2.5
	B2GP-PLYP	–1.5	0.5

[a]A positive value indicates the dispersion correction improves the performance of the functional, whereas a negative value indicates deterioration in performance.
[b]Footnote *a* to Table 1 applies here.

4. Conclusions

We introduce a representative benchmark database of eight C_{60} isomers to be known as the iso-C60 database. The reference energies are obtained at the CCSD(T) level by means of the G4(MP2) composite method. These benchmark values allow us to assess the performance of a variety of contemporary DFT, DHDFT, and MP2-based ab initio procedures. We considered a total of 115 methods: 12 GGA, 11 meta-GGA, 26 hybrid-GGA, 25 hybrid-meta-GGA, 17 range-separated, and 13 double-hybrid DFT methods; and 11 ab initio methods. With regard to the performance of the conventional DFT and DHDFT procedures we make the following observations:

- The average RMSD over the DFT functionals from each type are:
    - GGA: 27.5 kJ mol^{-1}
    - Meta-GGA: 23.0 kJ mol^{-1}
    - Hybrid-GGA: 71.4 kJ mol^{-1}
    - Hybrid-meta-GGA: 81.4 kJ mol^{-1}
    - Double-hybrid: 22.5 kJ mol^{-1}
- The best performing DFT functionals from each type are (RMSDs are given in parenthesis):
    - GGA: N12 (17.5), HCTH407 (20.3), BLYP-D3BJ (21.8 kJ mol^{-1})
    - Meta-GGA: TPSS-D3BJ (15.3), M06-L (17.7), M11-L (18.1), τ-HCTH (18.5), MN15-L (18.8 kJ mol^{-1})
    - Hybrid-GGA (not recommended): B3PW91-D3 (45.6 kJ mol^{-1})
    - Hybrid-meta-GGA: TPSSh-D3 (22.5 kJ mol^{-1})
    - Double-hybrid: B2T-PLYP (10.6), mPW2-PLYP (10.9), B2GP-PLYP (14.8), and B2K-PLYP (15.3 kJ mol^{-1})
- Overall, meta-GGA functionals show the best performance relative to computational cost.
- Inclusion of percentages of exact HF exchange beyond 5% results in sharp deterioration in performance.
- Empirical D3 and D3BJ dispersion corrections have a minor effect on performance.

With regard to the performance of MP2-based ab initio procedures, we draw the following conclusions:

- MP2 shows poor performance with an RMSD of 141.7 kJ mol^{-1}
- SCS-MP2 cuts this RMSD by 40% to 88.2 kJ mol^{-1}

- Optimizing the same-spin and opposite-spin scaling factors to minimize the RMSD over the iso-C60 dataset results in an RMSD of 20.9 kJ mol^{-1}. Thus, there is no advantage of using MP2-based methods over DHDFT or even simple GGA and meta-GGA functionals for the prediction of fullerene isomerization energies.

Supplementary data

Relative errors (Table S1) and error analysis (Table S2) for all 115 methods considered in the present work. Full references for the Gaussian and Molpro program suites (Table S3).

Acknowledgments

This research was undertaken with the assistance of resources from the National Computational Infrastructure (NCI), which is supported by the Australian Government. We also acknowledge the system administration support provided by the Faculty of Science at the University of Western Australia to the Linux cluster of the Karton group. AK gratefully acknowledges an Australian Research Council (ARC) Future Fellowship (Project No. FT170100373). SLW acknowledges a University of Newcastle Postgraduate Scholarship award.

References

[1] Sure, R.; Hansen, A.; Schwerdtfeger, P.; Grimme, S. Comprehensive theoretical study of all 1812 C_{60} isomers. *Phys. Chem. Chem. Phys.* **2017**, *19*, 14296–14305.

[2] Schwerdtfeger, P.; Wirz, L. N.; Avery, J. The topology of fullerenes. *WIREs Comput. Mol. Sci.*, **2015**, *5*, 96–145.

[3] Chan, B.; Kawashima, Y.; Katouda, M.; Nakajima, T.; Hirao, K. From C_{60} to Infinity: Large-Scale Quantum Chemistry Calculations of the Heats of Formation of Higher Fullerenes. *J. Am. Chem. Soc.* **2016**, *138*, 1420–1429.

[4] Wang, W.-W.; Dang, J.-S.; Zheng, J.-J.; Zhao, X.; Nagase, S. Selective Growth of Fullerenes from C_{60} to C_{70}: Inherent Geometrical Connectivity Hidden in Discrete Experimental Evidence, *J. Phys. Chem. C* **2013**, *117*, 2349–2357.

[5] Maroto, E. E.; Izquierdo, M.; Reboredo, S.; Marco-Martinez, J.; Filippone, S.; Martin, N. Chiral Fullerenes from Asymmetric Catalysis. *Acc. Chem. Res.* **2014**, *47*, 2660–2670.

[6] Raghavachari, K.; Rohlfing, C. M. Imperfect fullerene structures: isomers of C_{60}. *J. Phys. Chem.* **1992**, 96, 2463–2466.

[7] Perdew, J. P.; Schmidt, K. Jacob's ladder of density functional approximations for the exchange-correlation energy. *AIP Conf. Proc.* **2001**, 577, 1.

[8] Goerigk, L.; Hansen. A.; Bauer, C. A.; Ehrlich, S.; Najibi, A.; Grimme, S. A look at the density functional theory zoo with the advanced GMTKN55 database for general main group thermochemistry, kinetics and noncovalent interactions. *Phys. Chem. Chem. Phys.* **2017**, *19*, 32184–32215.

[9] Mardirossian, N.; Head-Gordon, M. Thirty years of density functional theory in computational chemistry: an overview and extensive assessment of 200 density functionals. *Mol. Phys.* **2017**, *115*, 2315–2372.

[10] Goerigk, L.; Grimme, S. Double-hybrid density functionals. *WIREs Comput. Mol. Sci.* **2014**, *4*, 576–600.

[11] Goerigk, L.; Grimme, S. A thorough benchmark of density functional methods for general main group thermochemistry, kinetics, and noncovalent interactions. *Phys. Chem. Chem. Phys.* **2011**, *13*, 6670–6688.

[12] Goerigk, L.; Grimme, S. Efficient and Accurate Double-Hybrid-Meta-GGA Density Functionals—Evaluation with the Extended GMTKN30 Database for General Main Group Thermochemistry, Kinetics, and Noncovalent Interactions, *J. Chem. Theory Comput.* **2011**, *7*, 291–309.

[13] Hujo, W.; Grimme, S. Performance of the van der Waals Density Functional VV10 and (hybrid)GGA Variants for Thermochemistry and Noncovalent Interactions. *J. Chem. Theory Comput.* **2011**, *7*, 3866–3871.

[14] Karton, A.; Goerigk, L. Accurate reaction barrier heights of pericyclic reactions: Surprisingly large deviations for the CBS-QB3 composite method and their consequences in DFT benchmark studies. *J. Comput. Chem.* **2015**, *36*, 622–632.

[15] Yu, L.-J.; Sarrami, F.; O'Reilly, R. J.; Karton, A. Reaction barrier heights for cycloreversion of heterocyclic rings: An Achilles' heel for DFT and standard ab initio procedures. *Chem. Phys.* **2015**, *458*, 1–8.

[16] Karton, A.; Daon, S.; Martin, J. M. L. W4-11: A high-confidence dataset for computational thermochemistry derived from W4 ab initio data. *Chem. Phys. Lett.* **2011**, *510*, 165–178.

[17] Karton, A. How reliable is DFT in predicting the relative energies of polycyclic aromatic hydrocarbon isomers? Comparison of functionals from different rungs of Jacob's Ladder. *J. Comput. Chem.* **2017**, *38*, 370–382.

[18] Yu, L.-J.; Karton, A. Assessment of theoretical procedures for a diverse set of isomerization reactions involving double-bond migration in conjugated dienes. *Chem. Phys.* **2014**, *441*, 166–177.

[19] Karton, A.; Martin, J. M. L. Explicitly correlated benchmark calculations on C_8H_8 isomer energy separations: How accurate are DFT, double-hybrid and composite ab initio procedures? *Mol. Phys.* **2012**, *110*, 2477–2491.

[20] Karton, A.; Martin, J. M. L. Atomization energies of the carbon clusters C_n (n = 2–10) revisited by means of W4 theory as well as density functional, G*n*, and CBS methods. *Mol. Phys.* **2009**, 107, 977–990.

[21] Curtiss, L. A.; Redfern, P. C.; Raghavachari, K. Gaussian-4 theory using reduced order perturbation theory. *J. Chem. Phys.* **2007**, 127, 124105.

[22] Curtiss, L. A.; Redfern, P. C.; Raghavachari, K. G*n* theory. *WIREs Comput. Mol. Sci.* **2011**, *1*, 810–825.

[23] Karton, A. A computational chemist's guide to accurate thermochemistry for organic molecules. *WIREs Comput. Mol. Sci.* **2016**, *6*, 292–310.

[24] Karton, A.; Martin, J. M. L. Explicitly correlated W*n* theory: W1-F12 and W2-F12. *J. Chem. Phys.* **2012**, *136*, 124114.

[25] Ramabhadran, R. O.; Raghavachari, K. Connectivity-Based Hierarchy for Theoretical Thermochemistry: Assessment Using Wave Function-Based Methods. *J. Phys. Chem. A* **2012**, *116*, 7531–7537.

[26] Wheeler, S. E.; Homodesmotic reactions for thermochemistry. *WIREs Comput. Mol. Sci.* **2012**, *2*, 204–220.

[27] Sarrami, F.; Yu, L.-J.; Karton, A. Thermochemistry of icosahedral closo-dicarboranes: A composite ab initio quantum-chemical perspective. *Can. J. Chem.* **2016**, *94*, 1082–1089.

[28] Grimme, S. Density functional theory with London dispersion corrections. *WIREs Comput. Mol. Sci.* **2011**, *1*, 211–228.

[29] Grimme, S.; Antony, J.; Ehrlich, S.; Krieg, H. A consistent and accurate ab initio parametrization of density functional dispersion correction (DFT-D) for the 94 elements H–Pu. *J. Chem. Phys.* **2010**, *132*, 154104.

[30] Grimme, S.; Ehrlich, S.; Goerigk, L. Effect of the damping function in dispersion corrected density functional theory. *J. Comput. Chem.* **2011**, *32*, 1456–1465.

[31] Becke, A. D.; Johnson, E. R. A density-functional model of the dispersion interaction. *J. Chem. Phys.* **2005**, *123*, 154101.

[32] Lee, C. ; Yang, W.; Parr, R. G. Development of the Colle-Salvetti correlation-energy formula into a functional of the electron density. *Phys. Rev. B* **1988**, *37*, 785.

[33] Becke, A. D. Density-functional exchange-energy approximation with correct asymptotic behavior. *Phys. Rev. A* **1988**, *38*, 3098.

[34] Grimme, S. Semiempirical GGA-type density functional constructed with a long-range dispersion correction. *J. Comput. Chem.* **2006**, *27*, 1787–1799.

[35] Boese, A. D.; Handy, N. C. A new parametrization of exchange–correlation generalized gradient approximation functionals. *J. Chem. Phys.* **2001**, *114*, 5497.

[36] Perdew, J. P.; Burke, K.; Ernzerhof, M. Generalized Gradient Approximation Made Simple, *Phys. Rev. Lett.* **1996**, *77*, 3865–3868.

[37] Perdew, J. P. Density-functional approximation for the correlation energy of the inhomogeneous electron gas, *Phys. Rev. B* **1986**, *33*, 8822.

[38] Perdew, J. P.; Chevary, J. A.; Vosko, S. H.; Jackson, K. A.; Pederson, M. R.; Singh, D. J.; Fiolhais, C. Atoms, molecules, solids, and surfaces: Applications of the generalized gradient approximation for exchange and correlation. *Phys. Rev.* B **1992**, *46*, 6671.

[39] Peverati, R.; Zhao, Y.; Truhlar, D. G. Generalized Gradient Approximation That Recovers the Second-Order Density-Gradient Expansion with Optimized Across-the-Board Performance. *J. Phys. Chem. Lett.* **2011**, *2*, 1991–1997.

[40] Peverati, R.; Truhlar, D. G. Exchange–Correlation Functional with Good Accuracy for Both Structural and Energetic Properties while Depending Only on the Density and Its Gradient. *J. Chem. Theory Comput.* **2012**, *8*, 2310–2319.

[41] Zhao, Y.; Truhlar, D. G. A new local density functional for main-group thermochemistry, transition metal bonding, thermochemical kinetics, and noncovalent interactions. *J. Chem. Phys.* **2006**, *125*, 194101.

[42] Tao, J. M.; Perdew, J. P.; Staroverov, V. N.; Scuseria, G. E. Climbing the density functional ladder: Nonempirical meta-generalized gradient approximation designed for molecules and solids. *Phys. Rev. Lett.* **2003**, *91*, 146401.

[43] Boese, A. D.; Handy, N. C. New exchange-correlation density functionals: The role of the kinetic-energy density. *J. Chem. Phys.* **2002**, *116*, 9559.

[44] van Voorhis, T.; Scuseria, G. E. A novel form for the exchange-correlation energy functional. *J. Chem. Phys.* **1998**, *109*, 400.

[45] Becke, A. D. Density-functional thermochemistry. IV. A new dynamical correlation functional and implications for exact-exchange mixing. *J. Chem. Phys.* **1996**, *104*, 1040.

[46] Peverati, R.; Truhlar, D. G. M11-L: A Local Density Functional That Provides Improved Accuracy for Electronic Structure Calculations in Chemistry and Physics. *J. Phys. Chem. Lett.* **2012**, *3*, 117–124.

[47] Peverati, R.; Truhlar, D. G. An improved and broadly accurate local approximation to the exchange-correlation density functional: the MN12-L functional for electronic structure calculations in chemistry and physics. *Phys. Chem. Chem. Phys.* **2012**, *10*, 13171–13174.

[48] Yu, H. S.; He, X.; Li, S. L.; Truhlar, D. G. MN15: A Kohn–Sham global-hybrid exchange–correlation density functional with broad accuracy for multi-reference and single-reference systems and noncovalent interactions. *Chem. Sci.* **2016**, *7*, 5032–5051.

[49] Becke, A. D. A new mixing of Hartree–Fock and local density-functional theories. *J. Chem. Phys.* **1993**, *98*, 1372.

[50] Becke, A. D. Density-functional thermochemistry. III. The role of exact exchange. *J. Chem. Phys.* **1993**, *98*, 5648.

[51] Stephens, P. J.; Devlin, F. J.; Chabalowski, C. F.; Frisch, M. J. Ab Initio Calculation of Vibrational Absorption and Circular Dichroism Spectra Using Density Functional Force Fields. *J. Phys. Chem.* **1994**, *98*, 11623–11627.

[52] Adamo, C.; Barone, V. Toward reliable density functional methods without adjustable parameters: The PBE0 model. *J. Chem. Phys.* **1999**, *110*, 6158.

[53] Hamprecht, F. A.; Cohen, A. J.; Tozer, D. J.; Handy, N. C. Development and assessment of

new exchange-correlation functionals. *J. Chem. Phys.* **1998**, *109*, 6264.

[54] Schmider, H. L.; Becke, A. D. Optimized density functionals from the extended G2 test set. *J. Chem. Phys.* **1998**, *108*, 9624.

[55] Xu, X.; Zhang, Q.; Muller, R. P.; Goddard, W. A. An extended hybrid density functional (X3LYP) with improved descriptions of nonbond interactions and thermodynamic properties of molecular systems. *J. Chem. Phys.* **2005**, *122*, 014105.

[56] Peverati, R.; Truhlar, D. G. Communication: A global hybrid generalized gradient approximation to the exchange-correlation functional that satisfies the second-order density-gradient constraint and has broad applicability in chemistry. *J. Chem. Phys.* **2011**, *135*, 191102.

[57] Austin, A.; Petersson, G.; Frisch, M. J.; Dobek, F. J.; Scalmani, G.; Throssell, K. A Density Functional with Spherical Atom Dispersion Terms. *J. Chem. Theory and Comput.* **2012**, *8*, 4989–5007.

[58] Adamo, C.; Barone, V. Exchange functionals with improved long-range behavior and adiabatic connection methods without adjustable parameters: The mPW and mPW1PW models. *J. Chem. Phys.* **1998**, *108*, 664.

[59] Heyd, J.; Scuseria, G. E.; Ernzerhof, M. Hybrid functionals based on a screened Coulomb potential. *J. Chem. Phys.* **2003**, *118*, 8207.

[60] Krukau, A. V.; Vydrov, O. A.; Izmaylov, A. F.; Scuseria, G. E. Influence of the exchange screening parameter on the performance of screened hybrid functionals. *J. Chem. Phys.* **2006**, *125*, 224106.

[61] Zhao, Y.; Schultz, N. E.; Truhlar, D. G. Exchange-correlation functional with broad accuracy for metallic and nonmetallic compounds, kinetics, and noncovalent interactions. *J. Chem. Phys.* **2005**, *123*, 161103.

[62] Zhao, Y.; Schultz, N. E.; Truhlar, D. G. Design of Density Functionals by Combining the Method of Constraint Satisfaction with Parametrization for Thermochemistry,

Thermochemical Kinetics, and Noncovalent Interactions. *J. Chem. Theory Comput.* **2006**, *2*, 364–382.

[63] Zhao, Y.; Truhlar, D. G. The M06 suite of density functionals for main group thermochemistry, thermochemical kinetics, noncovalent interactions, excited states, and transition elements: two new functionals and systematic testing of four M06-class functionals and 12 other functionals. *Theor. Chem. Acc.* **2008**, *120*, 215–241.

[64] Zhao, Y.; Truhlar, D. G. Exploring the Limit of Accuracy of the Global Hybrid Meta Density Functional for Main-Group Thermochemistry, Kinetics, and Noncovalent Interactions. *J. Chem. Theory Comput.* **2008**, *4*, 1849–1868.

[65] Boese, A. D.; Martin, J. M. L. Development of density functionals for thermochemical kinetics. *J. Chem. Phys.* **2004**, *121*, 3405.

[66] Staroverov, V. N.; Scuseria, G. E.; Tao, J.; Perdew, J. P. Comparative assessment of a new nonempirical density functional: Molecules and hydrogen-bonded complexes. *J. Chem. Phys.* **2003**, *119*, 12129.

[67] Zhao, Y.; Truhlar, D. G. Design of Density Functionals That Are Broadly Accurate for Thermochemistry, Thermochemical Kinetics, and Nonbonded Interactions. *J. Phys. Chem. A* **2005**, *109*, 5656–5667.

[68] Grimme, S. Semiempirical hybrid density functional with perturbative second-order correlation. *J. Chem. Phys.* **2006**, *124*, 034108.

[69] Schwabe, T.; Grimme, S. Towards chemical accuracy for the thermodynamics of large molecules: new hybrid density functionals including non-local correlation effects. *Phys. Chem. Chem. Phys.* **2006**, *8*, 4398–4401.

[70] Brémond, É.; Adamo, C. Seeking for parameter-free double-hybrid functionals: The PBE0-DH model. *J. Chem. Phys.* **2011**, *135*, 024106.

[71] Brémond, É.; Sancho-García, J. C.; Pérez-Jiménez, Á. J.; Adamo, C. Communication: Double-hybrid functionals from adiabatic-connection: The QIDH model. *J. Chem. Phys.* **2014**, *141*, 031101.

[72] Karton, A.; Tarnopolsky, A.; Lamere, J.–F.; Schatz, G. C.; Martin, J. M. L. Highly accurate first-principles benchmark datasets for the parametrization and validation of density functional and other approximate methods. Derivation of a robust, generally applicable, double-hybrid functional for thermochemistry and thermochemical kinetics. *J. Phys. Chem. A* **2008**, *112*, 12868–12886.

[73] Tarnopolsky, A.; Karton, A.; Sertchook, R.; Vuzman, D.; Martin, J. M. L. Double-hybrid functionals for thermochemical kinetics. *J. Phys. Chem. A* **2008**, *112*, 3–8.

[74] Kozuch, S.; Gruzman, D.; Martin, J. M. L. DSD-BLYP: A General Purpose Double Hybrid Density Functional Including Spin Component Scaling and Dispersion Correction. *J. Phys. Chem. C* **2010**, *114*, 20801–20808.

[75] Kozuch, S.; Martin, J. M. L. Spin-component-scaled double hybrids: An extensive search for the best fifth-rung functionals blending DFT and perturbation theory. *J. Comput. Chem.* **2013**, *34*, 2327–2344.

[76] Kozuch, S.; Martin, J. M. L. DSD-PBEP86: in search of the best double-hybrid DFT with spin-component scaled MP2 and dispersion corrections. *Phys. Chem. Chem. Phys.* **2011**, *13*, 20104–20107.

[77] Chai, J.–D.; Head-Gordon, M. Systematic optimization of long-range corrected hybrid density functionals. *J. Chem. Phys.* **2008**, *128*, 084106.

[78] Chai, J.–D.; Head-Gordon, M. Long-range corrected hybrid density functionals with damped atom-atom dispersion corrections. *Phys. Chem. Chem. Phys.* **2008**, *10*, 6615–6620.

[79] Peverati, R.; Truhlar, D. G. Improving the Accuracy of Hybrid Meta-GGA Density Functionals by Range Separation. *J. Phys. Chem. Lett.* **2011**, *2*, 2810–2817.

[80] Peverati, R.; Truhlar, D. G. Screened-exchange density functionals with broad accuracy for chemistry and solid-state physics. *Phys. Chem. Chem. Phys.* **2012**, *14*, 16187–16191.

[81] Yanai, T.; Tew, D.; Handy, N. A new hybrid exchange correlation functional using the Coulomb-attenuating method (CAM-B3LYP). *Chem. Phys. Lett.* **2004**, *393*, 51–57.

[82] Henderson, T. M.; Izmaylov, A. F.; Scalmani, G.; Scuseria, G. E. Can short-range hybrids describe long-range-dependent properties? *J. Chem. Phys.* **2009**, *131*, 044108.

[83] Vydrov, O. A.; Scuseria, G. E. Assessment of a long-range corrected hybrid functional. *J. Chem. Phys.* **2006**, *125*, 234109.

[84] Iikura, H.; Tsuneda, T.; Yanai, T.; Hirao, K. A long-range correction scheme for generalized-gradient-approximation exchange functionals. *J. Chem. Phys.* **2001**, *115*, 3540.

[85] Grimme, S. Improved second-order Møller–Plesset perturbation theory by separate scaling of parallel- and antiparallel-spin pair correlation energies. *J. Chem. Phys.* **2003**, *118*, 9095.

[86] Jung, Y.; Lochan, R. C.; Dutoi, A. D.; Head–Gordon, M. Scaled opposite-spin second order Møller–Plesset correlation energy: An economical electronic structure method. *J. Chem. Phys.* **2004**, *121*, 9793.

[87] Distasio, R. A.; Head–Gordon, M. Optimized spin-component scaled second-order Møller-Plesset perturbation theory for intermolecular interaction energies. *Mol. Phys.* **2007**, *105*, 1073–1083.

[88] Hill, J. G.; Platts, J. A. Spin-Component Scaling Methods for Weak and Stacking Interactions. *J. Chem. Theory Comput.* **2007**, *3*, 80–85.

[89] King, R. A. On the accuracy of spin-component-scaled perturbation theory (SCS-MP2) for the potential energy surface of the ethylene dimer. *Mol. Phys.* **2009**, *107*, 789–795.

[90] Fink, R. F. Spin-component-scaled Møller-Plesset (SCS-MP) perturbation theory: a generalization of the MP approach with improved properties. *J. Chem. Phys.* **2010**, *133*, 174113.

[91] Weigend, F.; Ahlrichs, R. Balanced basis sets of split valence, triple zeta valence and quadruple zeta valence quality for H to Rn: Design and assessment of accuracy. *Phys. Chem. Chem. Phys.* **2005**, *7*, 3297–3305.

[92] Werner, H.-J.; Knowles, P. J.; Knizia, G.; Manby, F. R.; Schutz, M.; Celani, P.; Korona, T.; Lindh, R.; Mitrushenkov, A.; Rauhut, G.; *et al.* MOLPRO (version 2012.1) is a package of ab initio programs. Available at: http://www.molpro.net.

[93] Werner, H.-J.; Knowles, P. J.; Knizia, G.; Manby, F. R.; Schutz, M. Molpro: a generalpurpose quantum chemistry program package. *WIREs Comput. Mol. Sci.* **2012**, *2*, 242-253.

[94] Gaussian 09, Revision A.02, Frisch, M. J.; Trucks, G. W.; Schlegel, H. B.; Scuseria, G. E.; Robb, M. A.; Cheeseman, J. R.; Scalmani, G.; Barone, V.; Petersson, G. A.; Nakatsuji, H.; *et al.* Gaussian, Inc., Wallingford CT, 2016.

Graphical TOC